AD-A158 408 A STATISTICAL STUDY OF SOLAR TYPE-III BURSTS AND AURORAL KILOMETRIC RADIA..(U) IOWA UNIV IOWA CITY DEPT OF PHYSICS AND ASTRONOMY W M FARRELL ET AL. MAR 85 UNCLASSIFIED U. OF IOWA-85-7 N00014-76-C-0016 F/G 4/1 NL 1/1

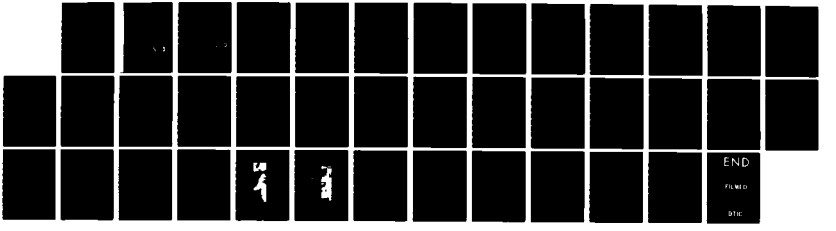

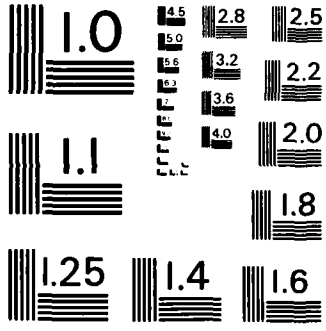

MICROCOPY RESOLUTION TEST CHART
NATIONAL BUREAU OF STANDARDS - 1963 - A

U. of Iowa 85-7

(1)

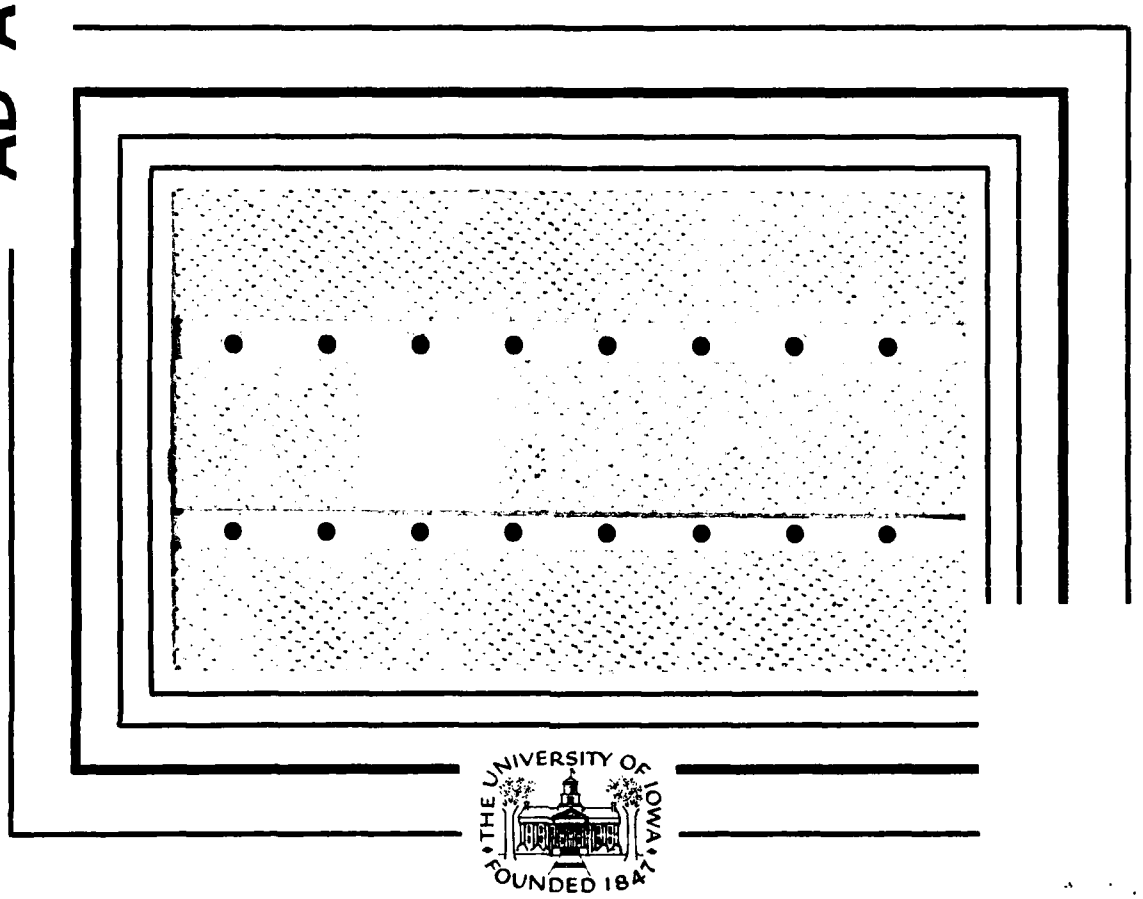

Department of Physics and Astronomy

THE UNIVERSITY OF IOWA

Iowa City, Iowa 52242

U. of Iowa 85-7

A STATISTICAL STUDY OF SOLAR TYPE-III BURSTS AND AURORAL KILOMETRIC RADIATION ONSETS

by

W. M. Farrell and D. A. Gurnett

March 1985

Department of Physics and Astronomy
The University of Iowa
Iowa City, Iowa 52242

The research at the University of Iowa was supported through contracts NAS5-26819 and NAS5-28701 with Goddard Space Flight Center, grants NGL-16-001-002 and NGL-16-001-04 with NASA Headquarters, and grant N00014-76-C-0016 with the Office of Naval Research.

SECURITY CLASSIFICATION OF THIS PAGE (When Data Entered)

REPORT DOCUMENTATION PAGE

READ INSTRUCTIONS BEFORE COMPLETING FORM

1. REPORT NUMBER: U. of Iowa 85-7	2. GOVT ACCESSION NO.: AD-A158 408
3. RECIPIENT'S CATALOG NUMBER:	
4. TITLE (and Subtitle): A Statistical Study of Solar Type-III Bursts and Auroral Kilometric Radiation Onsets	5. TYPE OF REPORT & PERIOD COVERED: Progress March 1985
	6. PERFORMING ORG. REPORT NUMBER:
7. AUTHOR(s): W. M. Farrell and D. A. Gurnett	8. CONTRACT OR GRANT NUMBER(s): N00014-76-C-0016
9. PERFORMING ORGANIZATION NAME AND ADDRESS: Department of Physics and Astronomy, University of Iowa, Iowa City, IA 52242	10. PROGRAM ELEMENT, PROJECT, TASK AREA & WORK UNIT NUMBERS:
11. CONTROLLING OFFICE NAME AND ADDRESS: Office of Naval Research, Electronics Program Office, Arlington, VA 22217	12. REPORT DATE: March 1985
	13. NUMBER OF PAGES: 36
14. MONITORING AGENCY NAME & ADDRESS (If different from Controlling Office):	15. SECURITY CLASS. (of this report): UNCLASSIFIED
	15a. DECLASSIFICATION/DOWNGRADING SCHEDULE:

16. DISTRIBUTION STATEMENT (of this Report)

Approved for public release; distribution is unlimited.

17. DISTRIBUTION STATEMENT (of the abstract entered in Block 20, if different from Report)

18. SUPPLEMENTARY NOTES

Submitted to J. Geophys. Res.

19. KEY WORDS (Continue on reverse side if necessary and identify by block number)

Auroral kilometric radiation
Type-III bursts

20. ABSTRACT (Continue on reverse side if necessary and identify by block number)

(See page following)

DD FORM JAN 73 1473 EDITION OF 1 NOV 65 IS OBSOLETE
S/N 0102-LF-014-6601

UNCLASSIFIED
SECURITY CLASSIFICATION OF THIS PAGE (When Data Entered)

ABSTRACT

Simultaneous occurrences of Type-III solar radio bursts and auroral kilometric radiation were observed by Calvert using ISEE-1 spectrograms. He presented evidence suggesting that the incoming Type-III burst stimulates the onset of auroral kilometric radiation.

This paper presents a statistical study of the correlation between Type-III bursts and auroral kilometric radiation. A superposed epoch analysis was performed on as many as 186 Type-III events. The Type-III bursts were detected by the ISEE-3 spacecraft on the sunward side of the earth. At the same time the IMP-8 spacecraft was used to detect onsets of kilometric radiation on the nightside of the earth. For each event, the intensities measured by ISEE-3 (Type-III intensities) were subtracted from the intensities measured by IMP-8 (Type-III and possible AKR intensities). The resulting intensities for each event were then added to determine if kilometric radiation was preferentially observed following a Type-III burst. This analysis was performed at frequencies of 100 kHz, 178 kHz and 500 kHz.

The results of this study show that a statistically significant correlation exists between incoming Type-III bursts from the sun and kilometric radiation from the earth.

I. INTRODUCTION

Calvert [1981a] presented evidence suggesting that Type-III solar radio bursts from the sun stimulate auroral kilometric radiation (AKR) from the earth. This paper presents a statistical study of the Type-III/AKR relationship using a superposed epoch analysis from a large sample of Type-III events. A comparison of pre-event and post-event intensities are made to determine if AKR is consistently triggered by Type-III radio bursts.

The earth is a strong source of radiation in the kilometric wavelength regime. This radiation is called auroral kilometric radiation. Auroral kilometric radiation is most intense at frequencies between 50-500 kHz [Dunkel et al., 1970; Gurnett, 1974] and is emitted from the auroral region between 1.4 and 3 R_e [Gurnett, 1974; Gallagher and Gurnett, 1979]. The emission tends to occur in intense bursts lasting a few hours with the intensity varying in both frequency and time. Gurnett [1974] found that most AKR occurrences are on the nightside of the earth (between 6 hour to 18 hour MLT) and that the radiation is emitted in a broad conical region centered on about 22 hours MLT. Hawkeye 1 [Gurnett and Green, 1978] and ISIS 1 [Benson and Calvert, 1979; Calvert, 1981b] data indicate that AKR is propagating in the free space R-X mode and is emitted nearly perpendicular to the magnetic field lines in the source

region. The source region also has a diminished plasma density [Calvert, 1981c] with the electron plasma frequency, f_{pe}, well below the electron gyrofrequency, f_{ge}.

Gurnett [1974] found that the occurrence of AKR is associated with discrete auroral arcs. These arcs are generated by intense beams of energetic (inverted-V) electrons moving along auroral magnetic field lines. The relationship of AKR to inverted-V electron precipitation has been confirmed by Benson et al. [1980]. Most AKR generation theories developed today make use of the free energy of the auroral electrons. Melrose [1976] suggests that the inverted-V electron beam amplifies low level radiation into AKR via the Doppler-shifted beam cyclotron resonance $\omega \cong n\omega_{ge} + k_{\parallel}v_b$. Wu and Lee [1979] suggest that part of the incoming inverted-V beam is absorbed by the atmosphere, thereby creating a loss cone in the reflected electron distribution. Using a relativistic cyclotron resonance, $\omega - k_{\parallel}v_{\parallel} = \omega_{ge}/\gamma$ where $\gamma = (1 - \frac{v^2}{c^2})^{-1/2}$, they show that the loss cone distribution produces an amplification of any low level radiation present in the source region. Omidi and Gurnett [1982] show positive growth rates in the AKR source region using the relativistic cyclotron resonance and measured S3-3 electron distribution functions.

Gurnett [1974] found that the maximum power output of AKR is on the order of 10^9 watts. Gallagher and Gurnett [1979] also found that the average power output of AKR is on the order of 10^7 watts. Both results indicate that the earth is a very intense radio source.

Based on current understanding, the auroral region with inverted-V electrons present acts much like a closed-loop amplifier in which the AKR can be triggered by weaker signals from internal or external sources. This feedback model of AKR generation, similar to an optical laser system, explains AKR's observed intensities, source locations, and fine structure [Calvert, 1982].

Solar flares often eject energetic particles into the solar wind. These streaming particles can be detected by satellite particle detectors well past 1 A.U. The electrons ejected from the flares have energies ranging from 1 keV to 100 keV and have electron velocities as high as 0.5 c.

The stream moving through the solar wind creates a bump-on-tail type electron distribution. Because fast particles arrive before the slow particles in any given location, the resulting electron beam is unstable and electron plasma oscillations develop at the local plasma frequency, f_{pe}. The electron plasma oscillations produce electromagnetic radiation (Type-III radiation) at f_{pe} and $2f_{pe}$ via a nonlinear process. For frequencies less than 1 MHz, the $2f_{pe}$ radiation appears to be the dominant component [Fainberg and Stone, 1974]. Since the plasma frequency, f_{pe}, decreases with increasing distance from the sun, a receiver will pick up a radio signal that drifts from high to low frequency with increasing time. This frequency drift is characteristic of Type-III bursts [Wild, 1950]. Figure 1 shows a Type-III burst detected by ISEE-1 that clearly illustrates the drift from high to low frequencies.

Solar Type-III bursts and AKR were believed to be unrelated phenomena until Calvert [1981a] noticed the simultaneous occurrence of the two emissions using ISEE-1 spectrograms. Figure 2 shows an example of simultaneous Type-III events and AKR bursts. Note that the start of two of the AKR events corresponds closely to the occurrence of Type-III bursts. This simultaneity led Calvert to believe that Type-III bursts stimulate AKR.

A model by Calvert suggests that Type-III radiation from the sun is refracted into the auroral zone by gradients in the plasma density. The radiation then passes through the AKR source region nearly perpendicular to the magnetic field. This incoming wave triggers AKR by exciting oscillations in the laser-like feedback system that generates AKR. Once triggered, the kilometric radiation can then persist long after the Type-III burst has ended.

Although Calvert's AKR stimulation model seems reasonable, another explanation is that the simultaneous occurrence of the two emissions is just an accidental temporal alignment. If this is the case, the probability of detecting an AKR onset should be the same whether a Type-III burst has occurred or not. Calvert did a study in which a number of independent, isolated Type-III bursts were examined for increased rates of AKR onsets after burst occurrences. ISEE-3, located at the L-1 lagrangian point on the sunward side of the earth at $\sim 200\ R_E$ was used to detect Type-III bursts independent of AKR (AKR occurs mainly on the nightside of earth). Corresponding ISEE-1 spectrograms were then checked for possible AKR onsets. Out

of 27 Type-III bursts checked, 8 showed AKR onsets within 30 minutes after the occurrence of a Type-III burst. In general, the average AKR onset rate per random 30-minute interval is 0.2 onsets per hour (or one AKR onset every 5 hours). The 30-minute interval after a Type-III event was more active with an AKR onset rate of 0.6 onsets per hour (i.e., 8/27 onsets in the 30-minute interval after the Type-III event). The increase in rate was attributed to Type-III stimulation of AKR [Calvert, 1981a]. Calvert's survey indicates that the simultaneity of Type-III bursts and AKR is not accidental, but is the result of a physical relationship between the two events.

In Calvert's survey, a certain amount of subjectivity is present in the identification of the AKR onset from ISEE-1 spectrogram inspection. One must first identify the onset, then check if it is within 30 minutes of a Type-III burst. Both identification and timing check are prone to human error.

This paper will present a survey in which Type-III bursts have been checked for AKR onsets using an automated superposed epoch analysis procedure. The value of this survey is that the processing was done entirely by a computer with no subjective judgement of AKR onsets. The survey made a comparison between the intensities of the isolated Type-III burst (detected by ISEE-3) and the corresponding intensities of possible Type-III triggered AKR (detected by IMP-8). This comparison was carried out at three frequencies: 100 kHz, 178 kHz, and 500 kHz.

II. SPACECRAFT INSTRUMENTATION

As mentioned, both the IMP-8 and ISEE-3 spacecraft were used in this study. The following is a brief sketch of the E-field detection devices on board each spacecraft.

The IMP-8 spacecraft is in a near equatorial earth orbit with a perigee radial distance of 147,343 km, an apogee radial distance of 295,054 km and an orbital period of 11.98 days. This orbit takes IMP-8 through regions where AKR can be detected (i.e., nightside of earth). The IMP-8 plasma wave experiment uses two electric dipole antennas (E_x and E_y) for E-field detection. The antennas were to have had a tip-to-tip length of 121.8m, but because of a mechanical failure only the E_y antenna extended to full length. Only data from the E_y antenna was used in this study. A fifteen channel spectrum analyzer is used to analyze the signals received from the antenna. This spectrum analyzer covers a frequency range of 40 Hz to 178 kHz with each channel being sampled every 10.24 seconds. In addition, a wideband receiver is available which can provide measurements over a frequency range from 10 Hz to 1 kHz. It can also be tuned to frequencies of 2.0 MHz, 500 kHz, 125 kHz, and 31.25 kHz. In this mode the receiver acts like another bandpass channel. For the period of time covering this survey, the wideband receiver was tuned to the 500-kHz channel. Measurements from the 100-kHz, 178-kHz and wideband

(500-kHz) frequency channels were used in this study since these frequencies correspond closely to the frequency range of AKR.

During this study, the ISEE-3 spacecraft was located near the L-1 Lagrangian point on the sunward side of the earth at a distance of about 200 R_E from the earth. From this position, ISEE-3 could easily detect Type-III radio bursts independent of AKR. The ISEE-3 three-dimensional radio mapping experiment and the ISEE-3 plasma wave experiment were used in this study. These two experiments were chosen because the frequency range of their E-field detection devices corresponds closely to the desired IMP-8 frequency channels.

The ISEE-3 radio mapping experiment uses two electric dipole antennas, one in the spacecraft spin plane (90m tip-to-tip) and one along the spin axis (15m tip-to-tip). These antennas are designated the S and Z antennas, respectively. The experiment is designed to study the coronal magnetic field and solar wind structure by tracking the trajectory of Type-III bursts. The modulation in intensity of the signal received by the S antenna can locate the azimuthal direction of arrival of a Type-III burst while signals from the S and Z antenna can locate the elevation. Each antenna drives two radiometers (one of 10-kHz bandwidth and one of 3-kHz bandwidth) and each radiometer steps through 12 frequencies (a different set of 12 for each radiometer) in a range from 30 kHz to 2 MHz [Knoll et al., 1978]. Of particular interest in this study were the S antenna

intensities measured at the 513-kHz and 188-kHz frequency channels. The measurements at these frequencies were compared to 500-kHz and 178-kHz IMP-8 channels.

The ISEE-3 plasma wave investigation uses the same antennas as the radio mapping experiment. Also, a search coil magnetometer is available to measure magnetic field strengths. The plasma wave investigation is designed to gain information on plasma wave-particle interactions. A 16-channel spectrum analyzer with a frequency range of 17 Hz to 100 kHz is used to analyze the signals received from the antennas. The analyzer can scan the frequency range every 0.5 seconds [Scarf et al., 1978]. The E-field measurements from the plasma wave experiment at 100 kHz were used in this study for comparison with the 100-kHz IMP-8 measurements.

Table 2. Second Hour Superposed Epoch Analysis Results

	$\bar{I}_{t>0}$ $(\frac{V}{m})^2 \frac{1}{Hz}$	$s_{t>0}$ $(\frac{V}{m})^2 \frac{1}{Hz}$	$SDM_{t>0}$ $(\frac{V}{m})^2 \frac{1}{Hz}$
100 kHz	5.13×10^{-15}	1.60×10^{-15}	$.48\times10^{-15}$
178 kHz	6.08×10^{-14}	2.78×10^{-14}	$.80\times10^{-14}$
500 kHz	18.34×10^{-18}	22.20×10^{-18}	5.83×10^{-18}

The average intensity, standard deviation, and standard deviation of the mean for $t < 0$, the first hour.

Table 1. First Hour Superposed Epoch Analysis Results

	$\bar{I}_{t<0}$ $(\frac{V}{m})^2 \frac{1}{Hz}$	$s_{t<0}$ $(\frac{V}{m})^2 \frac{1}{Hz}$	$SDM_{t<0}$ $(\frac{V}{m})^2 \frac{1}{Hz}$
100 kHz	6.04×10^{-15}	2.50×10^{-15}	$.75\times10^{-15}$
178 kHz	4.07×10^{-14}	1.07×10^{-14}	$.34\times10^{-14}$
500 kHz	4.74×10^{-18}	5.51×10^{-18}	2.08×10^{-18}

The average intensity, standard deviation, and standard deviation of the mean for $t < 0$, the first hour.

ACKNOWLEDGEMENTS

We are grateful to Bob Stone and Bob MacDowall for their ISEE-3 3-D radio mapping experiment data and to Fred Scarf for his ISEE-3 plasma wave investigation data. Terry Averkamp and Larry Granroth also deserve thanks for valuable input on data reduction and analysis. John Birkbeck deserves credit for a fine drafting job. Also, we would like to thank Wynne Calvert for very valuable comments and suggestions on this topic.

The research at the University of Iowa was supported through contracts NAS5-26819 and NAS5-28701 with Goddard Space Flight Center, grants NGL-16-001-002 and NGL-16-001-043 with NASA Headquarters, and grant N00014-76-C-0016 with the Office of Naval Research.

V. CONCLUSION

The superposed epoch analysis indicates that solar radio bursts affect the occurrence of auroral kilometric radiation. From the superposed epoch analysis, statistically significant intensity increases were observed at 178 kHz and 500 kHz after the occurrence of a Type-III burst. These intensity changes indicate an increase in AKR activity after the occurrence of Type-III bursts and imply that Type-III bursts affect the generation of AKR.

By noting the intensity change from first to second hour at 500 kHz, the AKR onset rate was seen to increase from .2 onsets/hour to .8 onsets/hour. The increased onset rate is attributed to Type-III triggered AKR and gives a result in close agreement to Calvert's results.

All of these conclusions confirm Calvert's hypothesis that incoming Type-III bursts stimulate AKR and show that an external (outside earth) source can cause AKR stimulation.

occurrence of the two emissions was not just an accident, but was the result of a cause-and-effect relationship.

As mentioned, $\overline{I}_{t<0}$ is a measure of all unrelated emissions found in the hourly period before incoming Type-III bursts. The first hour intensity, $\overline{I}_{t<0}$, includes the intensities of unrelated randomly occurring AKR. According to Calvert [1981a], the probability of obtaining a random AKR event is .2 onsets/hour. Since AKR was the strongest signal found on IMP-8 E-field detectors, $\overline{I}_{t<0}$ represents the measured intensity of the random occurring AKR. At 500 kHz, the intensity in the second hour was about four times greater than the first hour intensity. Assuming Type-III related AKR has the same intensities as randomly occurring AKR, this factor of four intensity increase implies an AKR onset rate of .8 onsets/hr in the second hour. The increased AKR activity was due to Type-III triggered AKR found in $t > 0$ and agrees quite nicely with Calvert's results of .6 AKR onsets per hour after Type-III burst passages.

that only unrelated radiation was detected. In order to explain the significantly large λ values, a Type-III/AKR correlation must exist with Type-III related AKR detected for $t > 0$. In other words, the statistically significant intensity increases are attributed to a Type-III/AKR correlation.

Looking at Figure 8, one sees that the bin intensities have relatively large fluctuations about $\bar{I}_{t<0}$ and $\bar{I}_{t>0}$. This result is not totally unexpected since it is AKR, with its large temporal fluctuations, that is being sampled. Even though one might suspect that the individual bin intensities vary to the extent of incompatibility, the individual bin standard deviations are relatively large and assure that all bin intensities are compatible.

Note from Figures 7 and 8 that the measured intensities in the second hour were remaining strong or even increasing in time even though normal Type-III burst intensities were decreasing. These observations indicates that the AKR events were not the result of a direct amplification of the Type-III bursts but rather resulted from a stimulation or triggering by the Type-III burst. If the process was of a direct amplification type, the strongest epoch analysis signals would have been seen from $t = 0$ to about $t = 30$ min. where the Type-III signal is largest. This process was not observed while the actual observed intensities indicate a triggering process.

The results at 178 kHz and 500 kHz, then, agree with Calvert's conclusion that Type-III bursts trigger AKR and that the simultaneous

values for H_0 true. One should note that Rosner's criteria for statistical significance is somewhat subjective. However, the completion of the hypothesis test required the selection of a p value and Rosner's criteria seemed adequate to solve the problem.

At 100 kHz, $\lambda < y_{.95}$ which means H_0 was accepted and $\bar{I}_{t>0} \cong \bar{I}_{t<0}$. Since no statistically significant increase in intensity was measured between the first and second hour, Type-III bursts did not affect AKR events at this frequency.

At 178 kHz, $\lambda > y_{.95}$ which means H_0 was rejected and H_1 accepted. This result indicates that a statistically significant intensity increase was measured between the first and second hours. The significant intensity increase in the second hour implies that a Type-III/AKR correlation exists at 178 kHz.

At 500 kHz, $\lambda > y_{.95}$ which means H_1 was accepted. This result again indicates that a statistically significant intensity increase had occurred between the first and second hour. The significant intensity increase in the second hour implies that a Type-III/AKR correlation exists at 500 kHz.

The probability of obtaining the intensity increases seen at 178 kHz and 500 kHz given that a Type-III/AKR correlation does not exist was calculated. This probability represents the likelihood that the unrelated radiation alone was the source of the intensity increases measured. The result of this calculation showed that the probability was less than .03 at both frequencies. Thus, the probability of obtaining this study's λ values at 178 kHz and 500 kHz was low given

Kilometric radiation was the strongest emission detected by IMP-8. It was often a factor of 10 to 100 times stronger than maximum Type-III burst intensities measured. Since AKR was the strongest signal measured in an event interval, the superposed epoch analysis is composed mostly of AKR signals found in all event intervals; other signals being to weak to contribute significantly.

As Figures 6, 7, and 8 show, the variance of the measurements changed from the first to the second hour. To compare $\overline{I}_{t<0}$ to $\overline{I}_{t>0}$, Cochran's approach to the Behrens-Fisher problem was used.

The standard deviation (s) and the standard deviation of the mean (SDM) for each hour were calculated. Table 1 shows the average intensity, s and SDM for the first hour. Table 2 shows the same quantities for the second hour. From the above quantities, it was possible to calculate λ, the test statistic. The test statistic λ was -1.03, 2.31 and 2.23 at 100 kHz, 178 kHz, and 500 kHz, respectively. A comparison of λ to y_{1-p} at a specific p-value was done to determine if hypothesis H_0 should have been accepted or rejected. According to Rosner [1982], λ has a statistically significant value if $\lambda > y_{.95}$ (i.e., λ has a statistically significant value if the probability of obtaining it, given H_0 is true, is less than .05). Thus, the hypothesis test consisted of comparing λ to $y_{.95}$. If $\lambda > y_{.95}$, hypothesis H_0 was rejected since this λ value was outside probable λ values for hypothesis H_0 true. The alternative hypothesis H_1 was accepted in this case. For $\lambda < y_{.95}$, hypothesis H_0 was accepted since λ was not statistically different from probable λ

IV. RESULTS

Figures 6, 7, and 8 show the results of the analysis at the 100 kHz, 178 kHz and 500 kHz frequency ranges. In these figures, the log of the spectral density is plotted vs. time, with t = 0 being the start of the Type-III burst. The line through the measurements represents the hourly averages, $\overline{I}_{t<0}$ and $\overline{I}_{t>0}$. At 100 kHz, no large intensity increase was found: the first hour average intensity (average of the unrelated radiation) was 6.04×10^{-15} $V^2m^{-2}Hz^{-1}$, while the second hour average intensity (average of the unrelated radiation plus any Type-III related AKR) was 5.12×10^{-15} $V^2m^{-2}Hz^{-1}$. At 178 kHz, an increase in intensity was clearly evident: the first hour average intensity was 4.07×10^{-14} $V^2m^{-2}Hz^{-1}$, while the second hour average intensity was 6.10×10^{-14} $V^2m^{-2}Hz^{-1}$. At 500 kHz, an even larger intensity increase was evident: the first hour average intensity was 4.7×10^{-18} $V^2m^{-2}Hz^{-1}$, while the second hour average intensity was 18.3×10^{-18} $V^2m^{-2}Hz^{-1}$. The number of Type-III events involved in the epoch analysis was 186 at 100 kHz and 140 at 178 kHz and 500 kHz.

Note, at 500 kHz, the background period picked was slightly less than an hour while the remaining period after t = 0 was slightly over an hour. This small time shift was the result of the earlier arrival of the Type-III bursts at 500 kHz which caused a shortening of the $t < 0$ period and a lengthening of the $t > 0$ period.

where $t_{\alpha,1-p}$ is the t-distribution value for statistical degree of freedom, α. The numbers α_1 and α_2 represent the statistical degrees of freedom for the first and second hours, respectively. By comparing λ to y_{1-p} for a specific probability, p, one can determine if a statistically significant intensity increase had occurred and determine which hypothesis should be accepted or rejected.

The superposed epoch analysis and hypothesis test were done at three different frequency ranges. The 100-kHz channel of IMP-8 was compared to the 100-kHz channel of ISEE-3, the 178-kHz channel of IMP-8 was compared with the 188-kHz channel of ISEE-3, and the 500-kHz channel of IMP-8 was compared with the 513-kHz channel of ISEE-3. It was assumed that Type-III intensities do not change substantially from 178 kHz to 188 kHz or from 500 kHz to 513 kHz.

Type-III/AKR correlation exists, one expected $\overline{I}_{t<0} = \overline{I}_{t>0}$. This result indicates that the second-hour intensities were derived from the same population as the first-hour intensities. If, however, AKR is triggered by Type-III bursts, a statistically significant increase in intensity should have occurred in the second hour ($\overline{I}_{t>0} > \overline{I}_{t<0}$). This result indicates the second-hour intensities were derived from a new population differing from the population of first-hour intensities. The problem, then, comes down to testing the hypothesis H_0: $\overline{I}_{t<0} = \overline{I}_{t>0}$ vs. H_1: $\overline{I}_{t>0} > \overline{I}_{t<0}$. In testing this hypothesis, it must be assumed that $SDM_{t<0}$ is not equal to $SDM_{t>0}$. This assumption is necessary since the possible presence of triggered AKR for $t > 0$ could cause $SDM_{t>0}$ to differ from $SDM_{t<0}$.

The problem of comparing two independent sample means that have unequal variances is known as the Behrens-Fisher problem [Rosner, 1982]. This problem is difficult to solve exactly, but one can use Cochran's approximation to determine which hypothesis is correct. In Cochran's approximation, a test statistic, $\lambda = (\overline{I}_{t>0} - \overline{I}_{t<0})/((SDM_{t<0})^2 + (SDM_{t>0})^2)^{1/2}$ is calculated. This test statistic λ is compared to a normalized t-distribution, y_{1-p}, where p is the probability of obtaining a value given that hypothesis H_0 is true. The normalized t-distribution, y_{1-p}, is defined as

$$y_{1-p} = \frac{(SDM_{t<0})^2 t_{\alpha_1,1-p} + (SDM_{t>0})^2 t_{\alpha_2,1-p}}{(SDM_{t<0})^2 + (SDM_{t>0})^2}$$

The IMP-8 intensity profile (with Type-III burst intensities subtracted) was added up, bin by bin, for all events. This procedure constitutes a superposed epoch analysis and yields a collective intensity profile that was made up of unrelated radiation and any Type-III related kilometric radiation. Once the epoch analysis was completed, the first hour overall intensity was statistically compared to the second hour overall intensity. This comparison determined if AKR was triggered by Type-III bursts.

The statistical analysis took the following steps:

1) Averages were computed for the first hour (the unrelated radiation) and second hour (the unrelated radiation and Type-III related AKR events) from the epoch analysis. The averages for the first and second hour are represented by $\overline{I}_{t<0}$ and $\overline{I}_{t>0}$, respectively.

2) The standard deviation of the mean (SDM) was calculated for the first and second hours. The SDM is defined as $s/\sqrt{n}$ where s is the sample standard deviation for n points. The distribution of the epoch analysis averages should approximate a normal distribution with a standard deviation equal to the SDM. The SDM for the first and second hour are represented by $SDM_{t<0}$ and $SDM_{t>0}$, respectively.

3) As mentioned, a comparison of $\overline{I}_{t<0}$ to $\overline{I}_{t>0}$ was done to test the hypothesis that AKR is triggered by Type-III bursts. It is assumed that the measured intensity samples that make up $\overline{I}_{t<0}$ belong to the population of unrelated, random occurring radiation. A comparison of the one-hour averages determined if the second-hour intensities belong to the same population as the first-hour intensities. Basically, if no

corresponding bin average intensities measured by IMP-8. In effect, the Type-III intensities measured by ISEE-3 were subtracted from the combined Type-III/AKR intensities measured by IMP-8. Thus, the subtracted intensities should represent that of any unrelated radiation plus any Type-III related AKR (found in $t > 0$) for each two-hour event interval.

Since the spectral density measurements of ISEE-3 were subtracted from the spectral density measurements of IMP-8, it is very important to verify the intensity calibration of both E-field detection instruments. To verify the calibration, the spectral density of an isolated Type-III event (without AKR onsets) measured with IMP-8 was compared to the spectral density of that same event measured with ISEE-3. If the intensity calibrations on both satellites are correct, the ratio of intensities of the Type-III burst (with the pre-event background subtracted) should be almost unity. The intensities measured by each satellite are compared by plotting the intensities on a log-log plot. Figures 3, 4, and 5 show this comparison at each frequency. Figure 3 shows the comparison of intensities for an isolated Type-III event on Sept. 6, 1978, at 5:59 UT for 100 kHz. Figure 4 and Figure 5 show the comparison of intensities for an isolated Type-III event on June 26, 1979, at 14:55 UT for 178 kHz and 500 kHz. Note that the ratio of intensities is close to unity. The best fit linear relationship between the points is shown by the straight line. These plots (and others like them) confirm that ISEE-3 and IMP-8 measure essentially the same intensities, in most cases within $\pm 5\%$.

III. ANALYSIS PROCEDURE

The first step in this study was to randomly select a set of Type-III bursts. Using the ISEE-3 survey data, independent Type-III bursts were selected with the following criterion: (1) that the burst was isolated (i.e., no strong interferring signals 1 hour before or after the burst); and (2) that IMP-8 was on the nightside of the earth (between 6 hours and 18 hours MLT) while the burst occurred. This last condition enhanced the likelihood of detecting stimulated AKR.

The start of each Type-III burst was defined as t = 0 for each of the three frequencies measured. The spectral density was then examined 1 hour before and 1 hour after t = 0 for events detected by both ISEE-3 and IMP-8. As mentioned, the ISEE-3 spacecraft is expected to detect only isolated Type-III burst intensities in the two-hour event interval. However, IMP-8 is expected to detect three types of radiation in the two-hour event interval: Type-III burst intensities, any Type-III related AKR, and also unrelated signals (presumably unrelated AKR).

The two-hour event interval was divided into equally spaced time bins. An average intensity for each time bin was then computed for measurements made by both ISEE-3 and IMP-8. For each event, the bin average intensities measured by ISEE-3 were subtracted from the

REFERENCES

Benson, R. F., and W. Calvert, ISIS-1 observations at the source of auroral kilometric radiation, Geophys. Res. Lett., 6, 479-482, 1979.

Benson, R. F., W. Calvert, and D. M. Klumpar, Simultaneous wave and particle observations in the auroral kilometric radiation source region, Geophys. Res. Lett., 7, 959-962, 1980.

Calvert, W., The stimulation of auroral kilometric radiation by Type-III solar radio bursts, Geophys. Res. Lett., 8, 1091, 1981a.

Calvert, W., The signature of auroral kilometric radiation on ISIS-1 ionograms, J. Geophys. Res., 86, 76-82, 1981b.

Calvert, W., The auroral plasma cavity, Geophys. Res. Lett., 8, 919, 1981c.

Calvert, W., A feedback model for the source of auroral kilometric radiation, J. Geophys. Res., 87, 8199-8214, 1982.

Dunckel, N., B. Ficklin, L. Rorden, and R. A. Helliwell, Low-frequency noise observed in the distant magnetosphere with OGO-1, J. Geophys. Res., 75, 1854-1862, 1970.

Fainberg, J., and R. G. Stone, Satellite observations of Type-III solar radio bursts at low frequencies, Space Sci. Rev., 16, 145-188, 1974.

Gallagher, D. L., and D. A. Gurnett, Auroral kilometric radiation: Time-averaged source location, J. Geophys. Res., 84, 6501-6509, 1979.

Gurnett, D. A., The earth as a radio source: Terrestrial kilometric radiation, J. Geophys. Res., 79, 4227-4238, 1974.

Gurnett, D. A., and J. L. Green, On the polarization and origin of auroral kilometric radiation, J. Geophys. Res., 83, 689-696, 1978.

Knoll, R., G. Epstein, S. Hoang, G. Huntzinger, J. L. Steinberg, J. Fainberg, F. Grena, S. R. Mosier, and R. G. Stone, The 3-dimensional radio mapping experiment (SBH) on ISEE-C, IEEE Trans. Geosci. Electron., GE-16, 199-204, 1978.

Lin, R. P., D. W. Potter, D. A. Gurnett, and F. L. Scarf, Energetic electrons and plasma waves associated with a solar Type-III radio burst, Astrophys. J., 251, 364-373, 1981.

Melrose, D. B., An interpretation of Jupiter's decametric radiation and the terrestrial kilometric radiation as direct amplified gyroemission, Astrophys. J., 207, 651, 1976.

Omidi, N., and D. A. Gurnett, Growth rate calculations of auroral kilometric radiation using the relativistic resonance condition, J. Geophys. Res., 87, 2377-2383, 1982.

Rosner, B., Fundamentals of Biostatistics, Durbury Press, Boston, Massachusetts, 1982.

Scarf, F. L., R. W. Fredricks, D. A. Gurnett, and E. J. Smith, The ISEE-C plasma wave investigation, IEEE Trans. Geosci. Electron., GE-16, 191-195, 1978.

Wild, J. P., Observations of the spectrum of high-intensity solar radiation at metre wavelengths, Aust. J. Sci., 3, 541-577, 1950.

Wu, C. S., and L. C. Lee, A theory of the terrestrial kilometric radiation, Astrophys. J., 230, 621-626, 1979.

FIGURE CAPTIONS

Figure 1 — An ISEE-1 spectrogram showing a Type-III burst occurring on November 17, 1979. Note the high to low frequency drift.

Figure 2 — An ISEE-1 spectrogram showing Type-III bursts and simultaneous AKR occurrences at 1630 and 2200 UT (from Calvert [1982]).

Figure 3 — The IMP-8 spectral density is compared to the ISEE-3 spectral density for the isolated Type-III burst occurring on Sept. 6, 1978, at 5:59 UT at 100 kHz.

Figure 4 — The IMP-8 spectral density is compared to the ISEE-3 spectral density for the isolated Type-III burst occurring on June 26, 1979, at 14:55 UT at 178 kHz.

Figure 5 — The IMP-8 spectral density is compared to the ISEE-3 spectral density for the isolated Type-III burst occurring on June 26, 1979, at 14:55 UT at 500 kHz.

Figure 6 The results of the superposed epoch analysis at 100-kHz are shown. The t = 0 point represents the start of the Type-III burst's passage for all events.

Figure 7 The results of the superposed epoch analysis at 178-kHz are shown. The t = 0 point represents the start of the Type-III burst's passage for all events.

Figure 8 The results of the superposed epoch analysis at 500-kHz are shown. The t = 0 point represents the start of the Type-III burst's passage for all events.

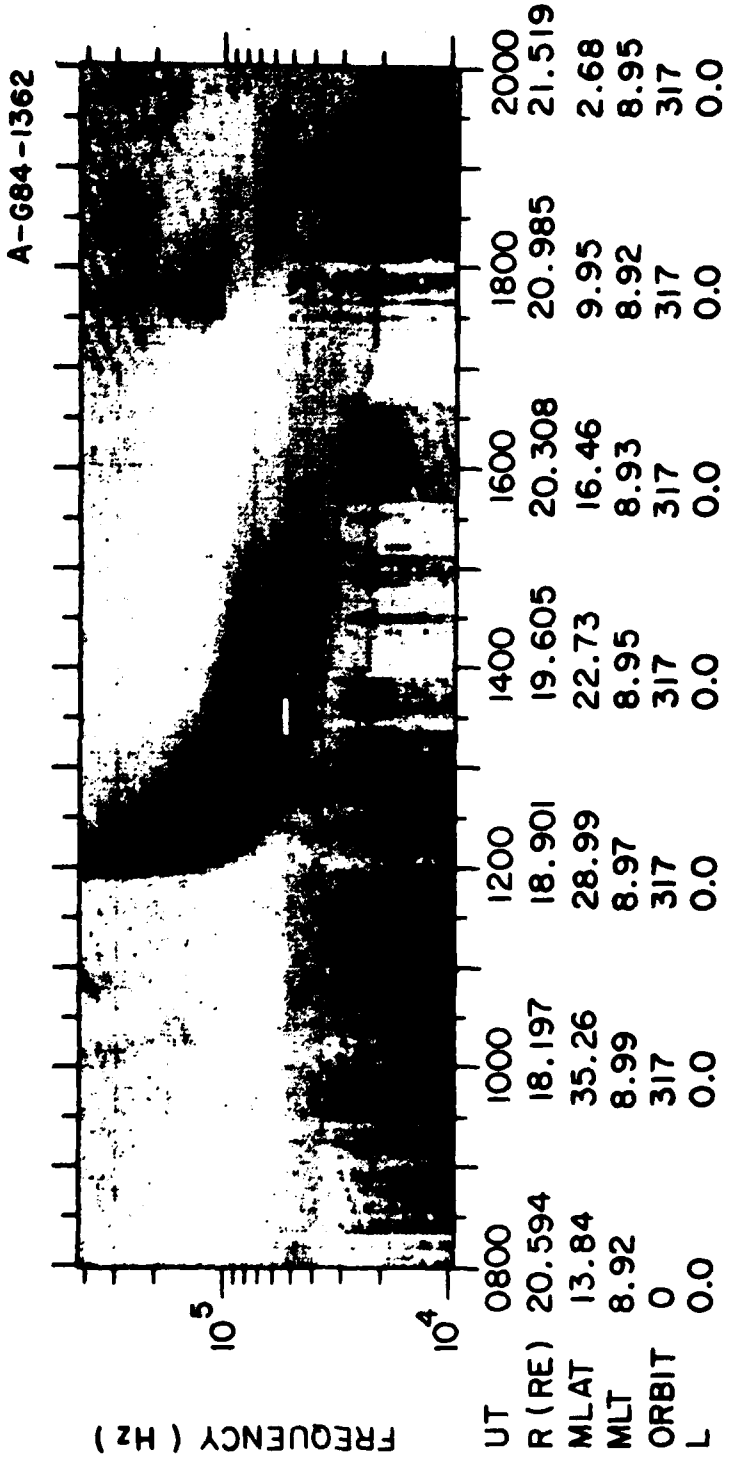
A-G84-1362
FREQUENCY (Hz)
10^5
10^4
UT 0800 1000 1200 1400 1600 1800 2000
R (RE) 20.594 18.197 18.901 19.605 20.308 20.985 21.519
MLAT 13.84 35.26 28.99 22.73 16.46 9.95 2.68
MLT 8.92 8.99 8.97 8.95 8.93 8.92 8.95
ORBIT 0 317 317 317 317 317 317
L 0.0 0.0 0.0 0.0 0.0 0.0 0.0

Figure 1

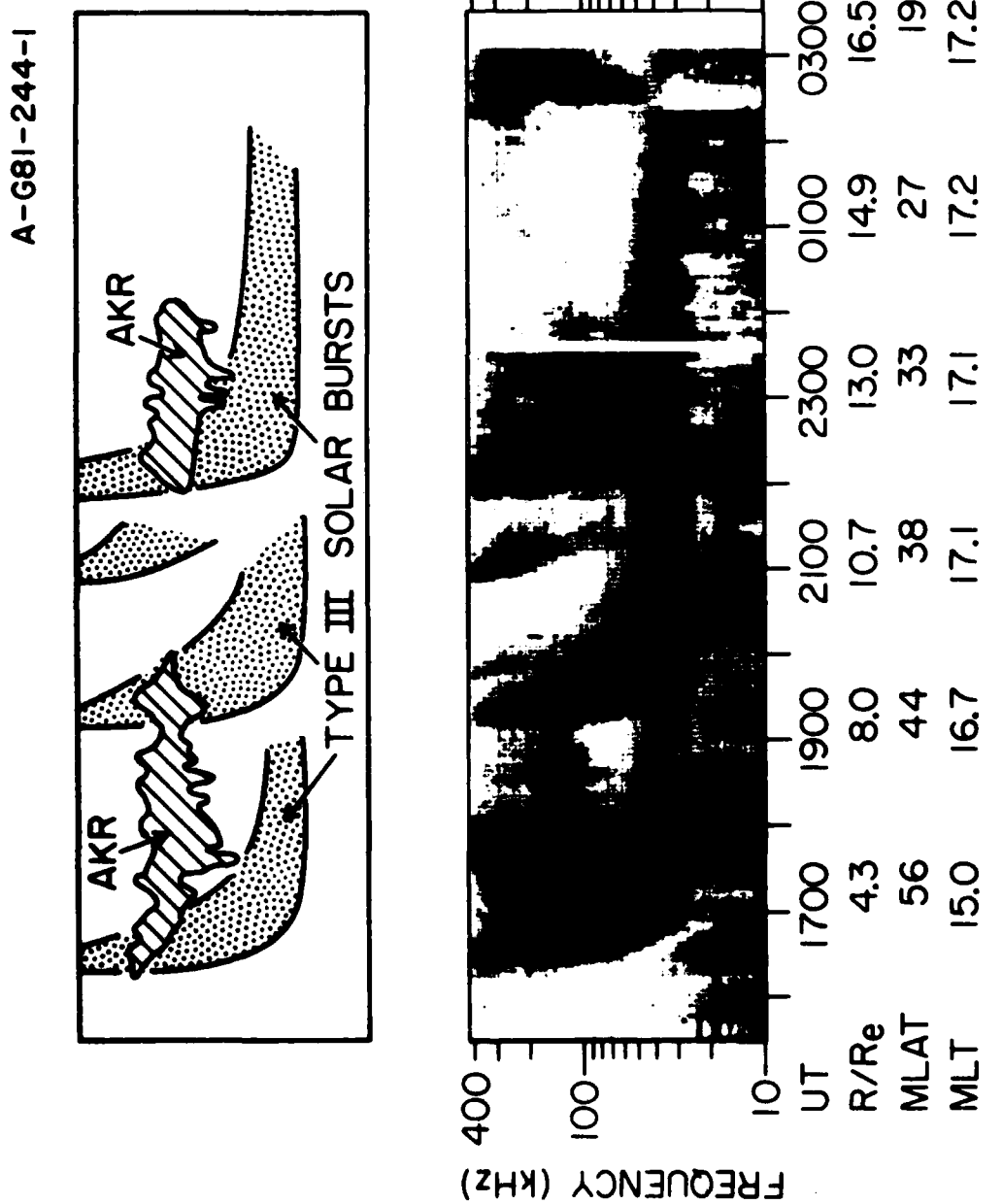
A-G81-244-1
AKR
AKR
TYPE III SOLAR BURSTS
FREQUENCY (kHz)
400
100
10
UT 1700 1900 2100 2300 0100 0300
R/Re 4.3 8.0 10.7 13.0 14.9 16.5
MLAT 56 44 38 33 27 19
MLT 15.0 16.7 17.1 17.1 17.2 17.2
ISEE-1 3-4 JULY 1979

Figure 2

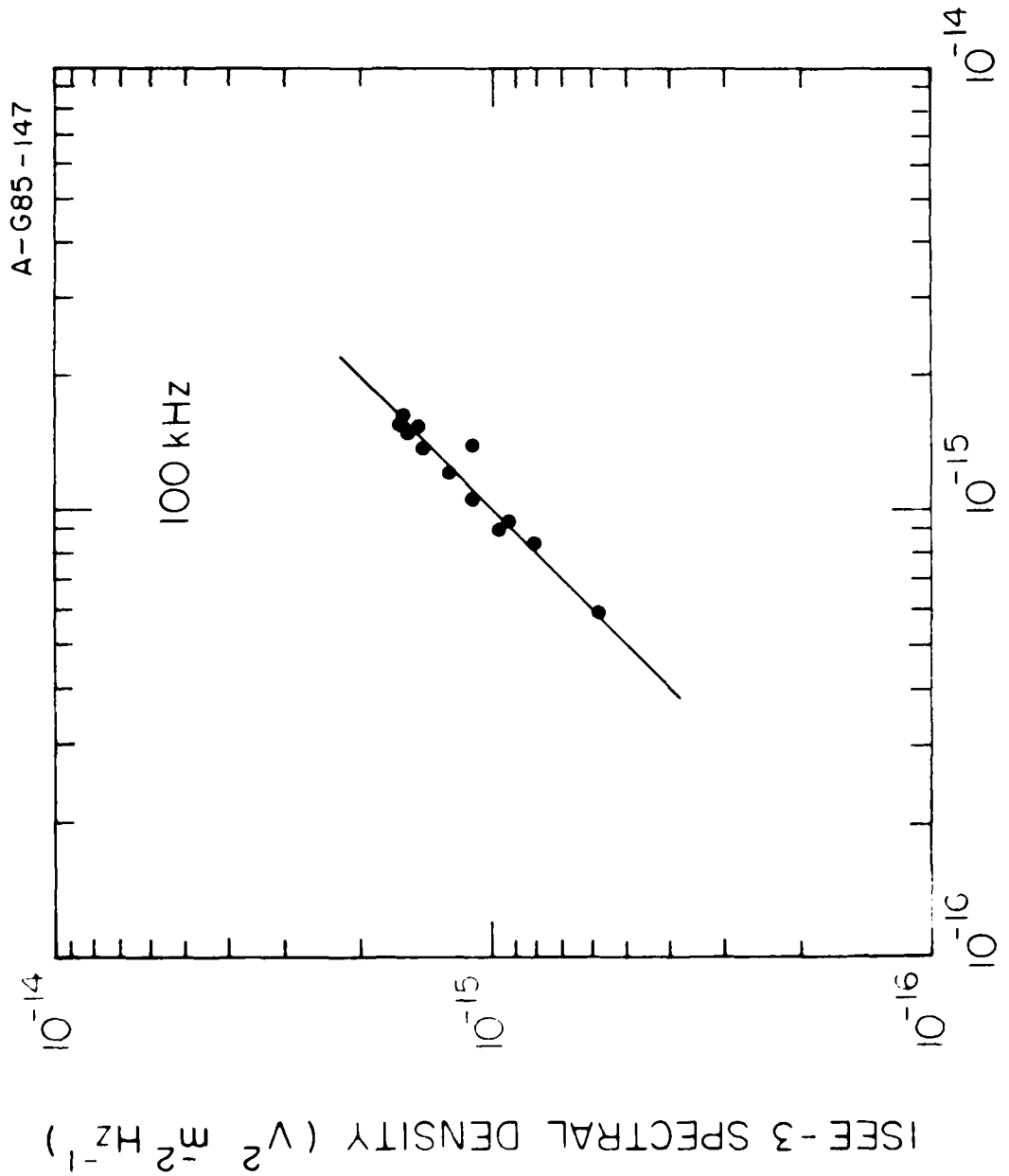
A-G85-147
100 kHz
10^{-14}
10^{-15}
10^{-16}
IMP-8 SPECTRAL DENSITY ($V^2 m^{-2} Hz^{-1}$)
ISEE-3 SPECTRAL DENSITY ($V^2 m^{-2} Hz^{-1}$)

Figure 3

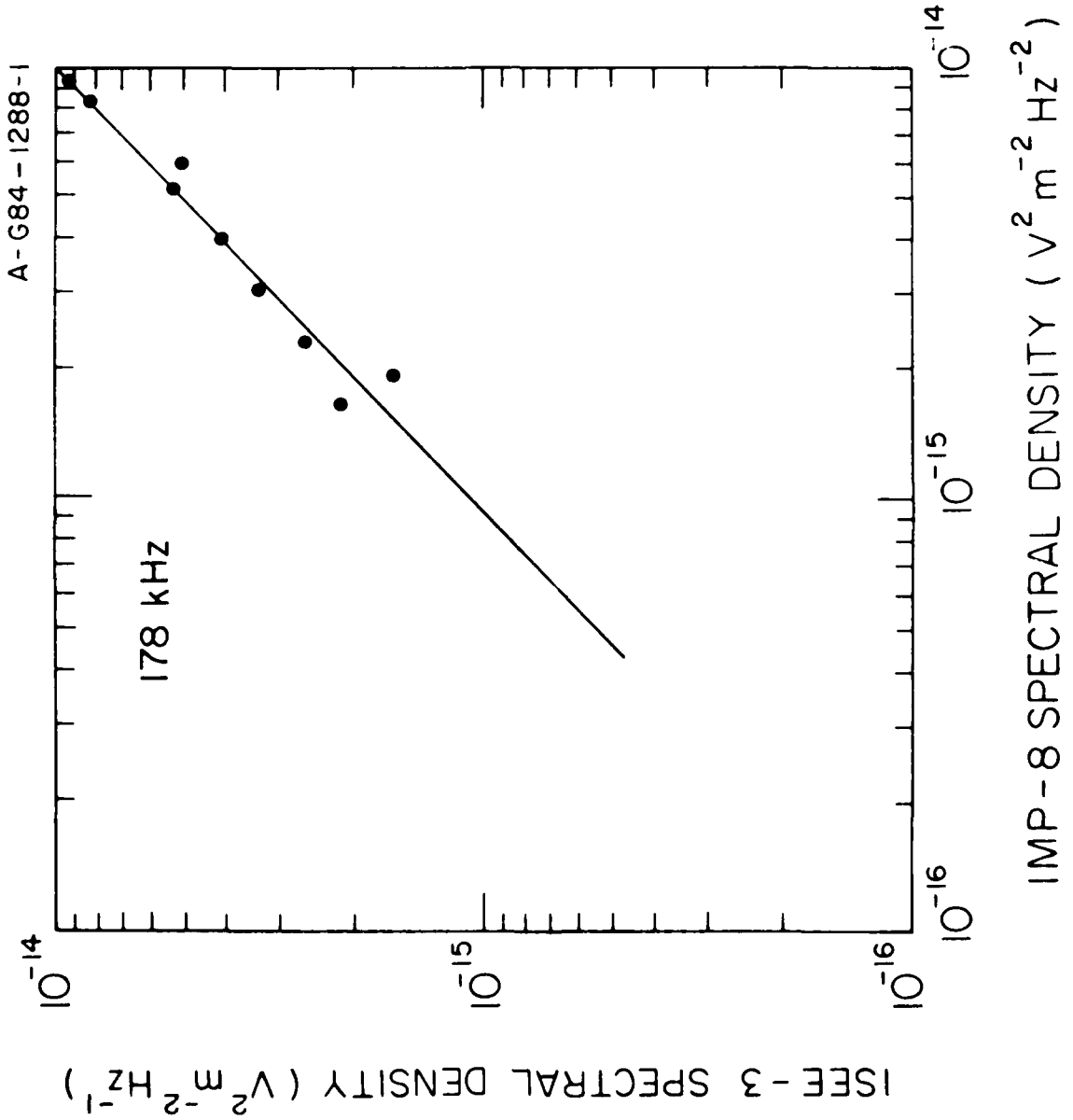
A-G84-1288-1
178 kHz
10^{-14}
10^{-15}
10^{-16}
ISEE-3 SPECTRAL DENSITY ($V^2 m^{-2} Hz^{-1}$)
IMP-8 SPECTRAL DENSITY ($V^2 m^{-2} Hz^{-2}$)

Figure 4

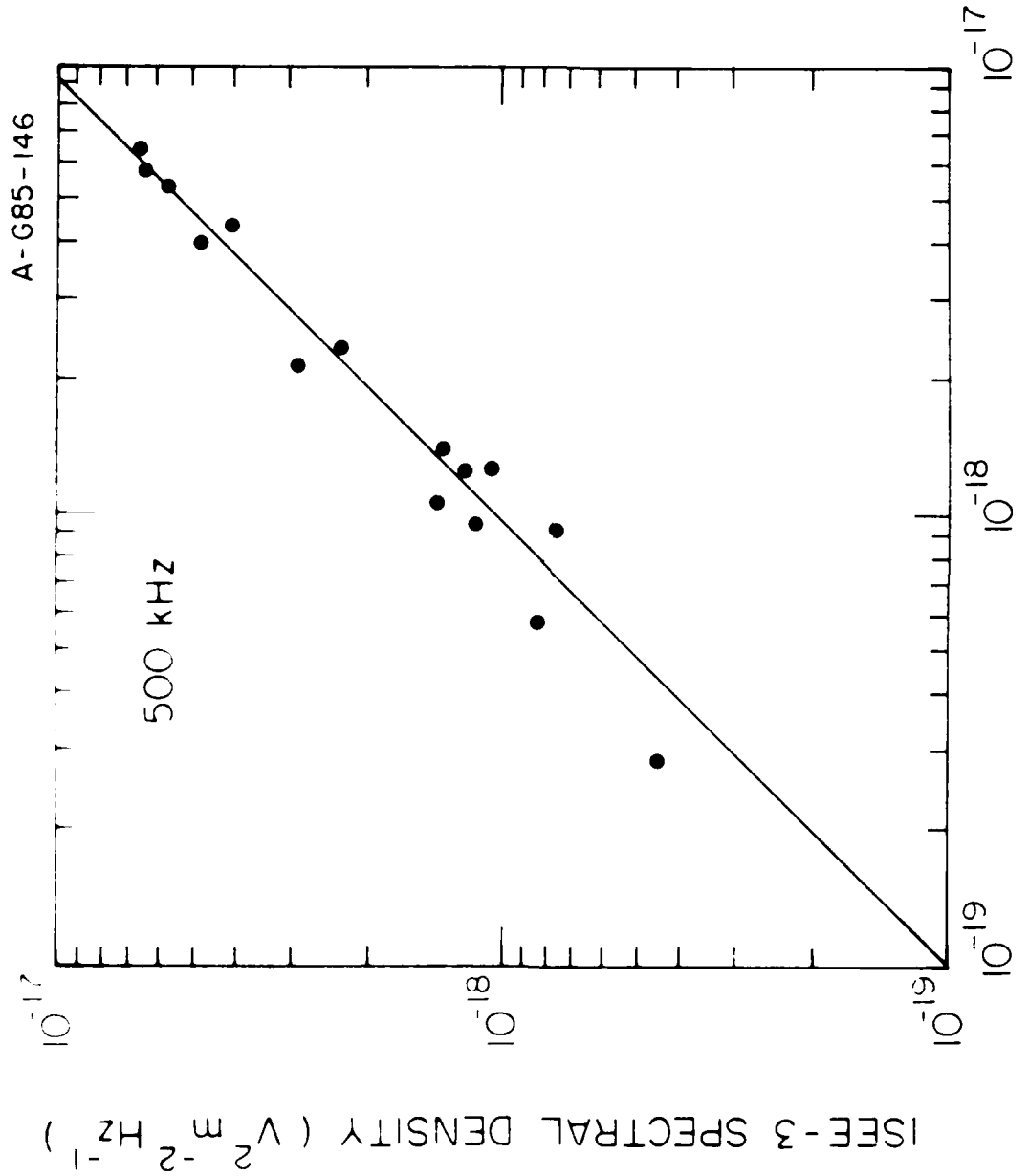
A-G85-146
500 kHz
ISEE-3 SPECTRAL DENSITY ($V^2 m^{-2} Hz^{-1}$)
IMP-8 SPCTRAL DENSITY ($V^2 m^{-2} Hz^{-1}$)
10^{-17}
10^{-18}
10^{-19}

Figure 5

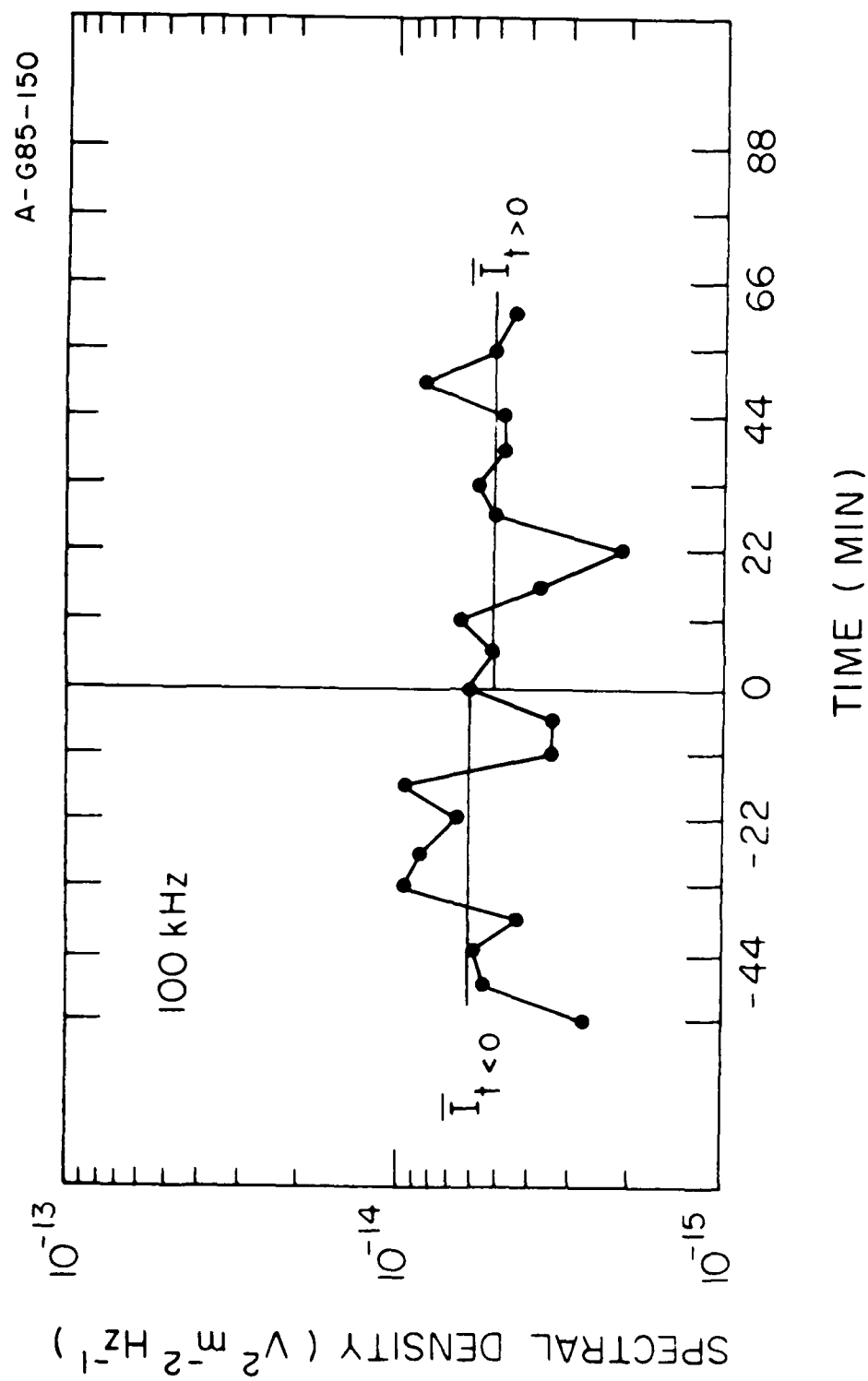
A-G85-150
100 kHz
$\overline{I}_{t<0}$
$\overline{I}_{t>0}$
10^{-13}
10^{-14}
10^{-15}
SPECTRAL DENSITY ($V^2 m^{-2} Hz^{-1}$)
-44
-22
0
22
44
66
88
TIME (MIN)

Figure 6

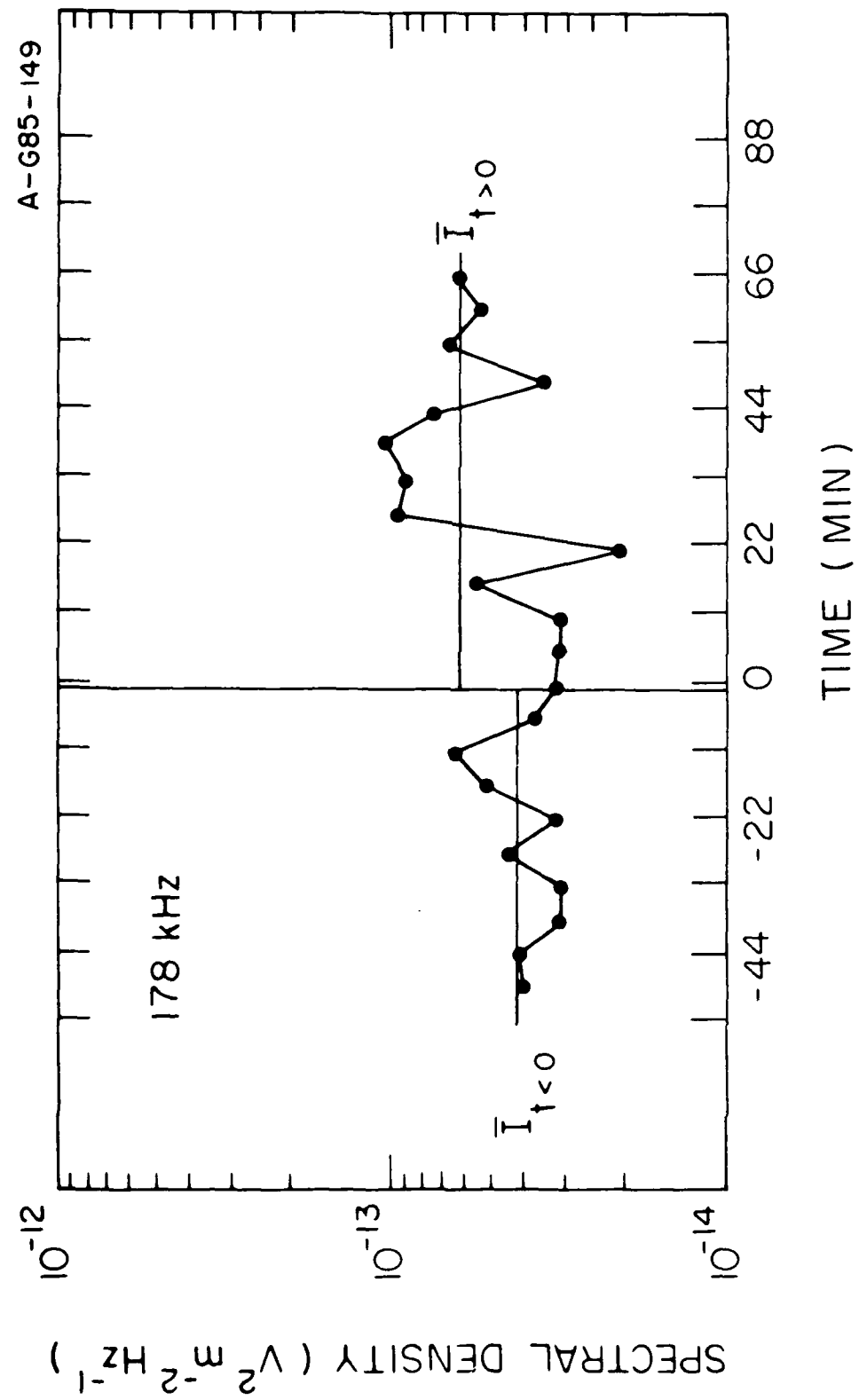
A-G85-149
178 kHz
$\bar{I}_{t<0}$
$\bar{I}_{t>0}$
10^{-12}
10^{-13}
10^{-14}
-44
-22
0
22
44
66
88
TIME (MIN)
SPECTRAL DENSITY ($V^2 m^{-2} Hz^{-1}$)

Figure 7

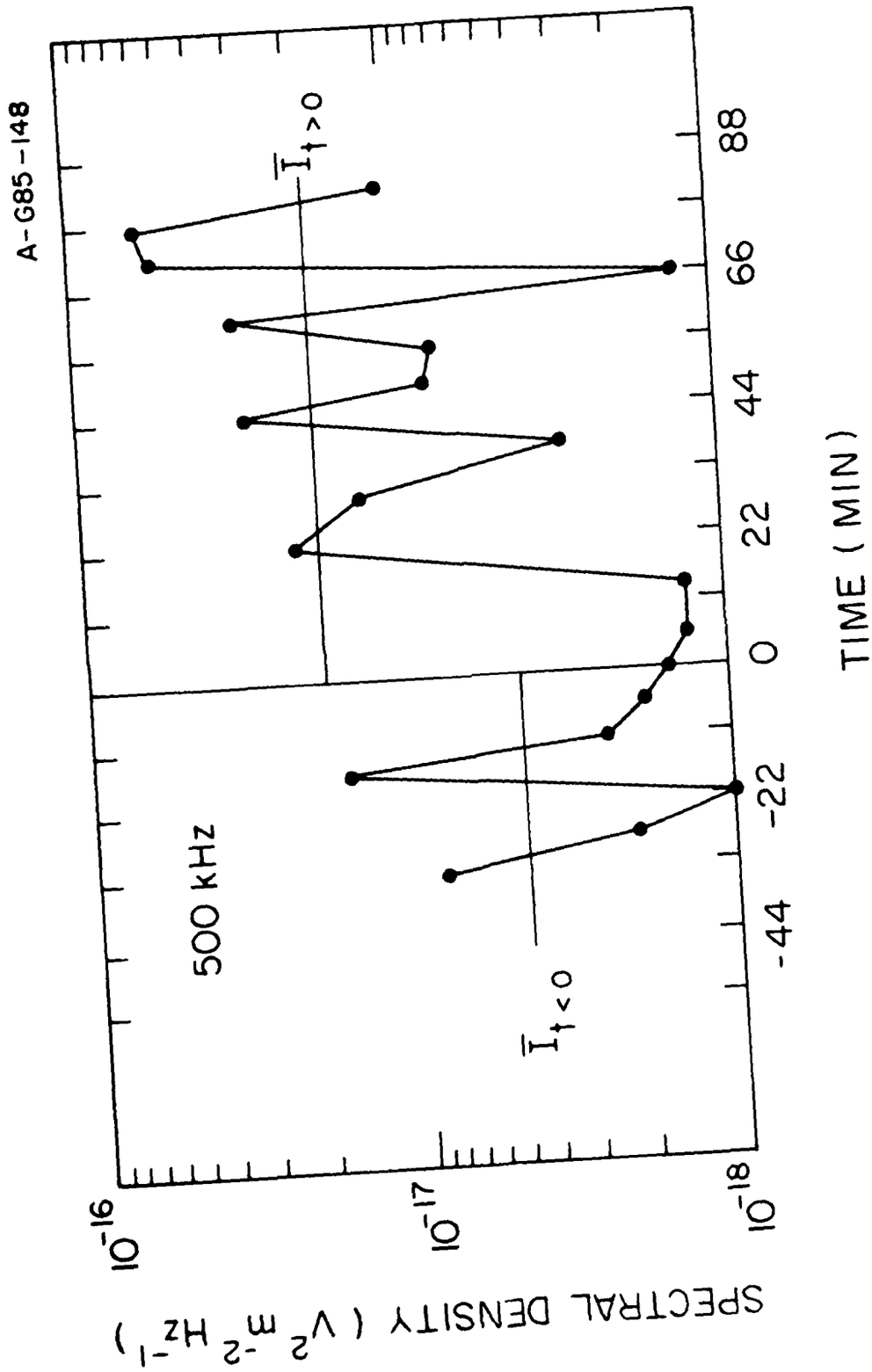
A-G85-148
500 kHz
$\bar{I}_{t>0}$
$\bar{I}_{t<0}$
10^{-16}
10^{-17}
10^{-18}
SPECTRAL DENSITY ($V^2 m^{-2} Hz^{-1}$)
88
66
44
22
0
-22
-44
TIME (MIN)

Figure 8

END

FILMED

10-85

DTIC